

# Virialisation of Galaxy Clusters in Numerical Simulations

Alexander Knebe

*Astrophysikalisches Institut Potsdam, An der Sternwarte 16, D-14482 Potsdam,  
Germany*

Numerical simulations of variants of the CDM model with different cosmological parameters are used to compare statistical measures such as mass spectra, merger processes, and autocorrelation functions, for different models with relevant observations. The degree of virialisation of the halos is checked, and also which properties distinguish recent mergers. Mergers occur mostly in deep potential wells and mark the most important structure formation processes. As consequence, the autocorrelation function of merged halos has a higher amplitude and is steeper than that of the virialized clusters. This effect can also be seen for ultraluminous IRAS galaxies which are thought to be results from ongoing merging events.

## 1 Introduction

Gravitational instability is accepted to be the basic driving agent of structure formation on large scales. Combined with the CDM model it leads to the picture of hierarchical clustering with wide support from deep galaxy and cluster observations. The most massive virialized objects we observe in the universe are clusters of galaxies. We can derive lots of cosmological information by investigating these objects in detail: Since they are just in the process of rising from rare high peaks in the primordial density field, non-linear effects have not erased all the information about their formation. Additionally the mass and abundance of galaxy clusters gives us a hint what the amplitude of the fluctuations in the primordial density field had been.

In order to derive reliable physical properties of galaxy clusters from numerical simulations one has to use large simulation boxes and a high resolution  $N$ -body code, because the overall large scale structure is connected to the sub-structure of halos (Colberg et al.1997).

## 2 Cosmological models

We base our analysis on three cosmological models all with an amplitude as determined by the 4-year COBE experiment, cp. Bunn & White (1997). First we take the standard CDM-model, with critical mass density  $\Omega_0 = 1$  and a dimensionless Hubble constant  $h = 0.5$ , which is used as a reference in spite of the difficulty in reproducing both large scale and small scale clustering. More realistic variants of the CDM model have a lower matter content, as

Table 1: Physical properties of the numerical simulations. The box size  $L$  is given in  $h^{-1}\text{Mpc}$ , the particle mass  $m_p$  in units of  $10^{11} h^{-1}M_\odot$ .

|                                | $\Omega_0$ | $\lambda_0$ | $\Gamma$ | $h$ | $\sigma_8$ | $L$ | $m_p$ |
|--------------------------------|------------|-------------|----------|-----|------------|-----|-------|
| <b>SCDM</b>                    | 1.0        | 0.0         | 0.5      | 0.5 | 1.18       | 200 | 11.0  |
| <b><math>\Lambda</math>CDM</b> | 0.3        | 0.7         | 0.21     | 0.7 | 1.00       | 280 | 8.7   |
| <b>OCDM</b>                    | 0.5        | 0.0         | 0.35     | 0.7 | 0.96       | 280 | 15.0  |

$\Lambda$ CDM which has  $\Omega_0 = 0.3$ , a cosmological constant of  $\lambda_0 = 0.7$ , and  $h = 0.7$ . For this model the shape parameter of the power spectrum  $\Gamma \equiv \Omega_0 h = 0.21$  better fits the constraints from galaxy and cluster clustering, (e.g. Peacock & Dodds 1996, Einasto et al.1998). The models were normalized to the full 4-year COBE anisotropy using the Boltzmann code CMBFAST developed by Seljak & Zaldarriaga (1996) and assuming a baryon content of  $\Omega_b h^2 = 0.0125$  suggested by big bang nucleosynthesis. The mass variance of the linear input spectrum at a scale of  $8h^{-1}\text{Mpc}$  is given by  $\sigma_8$ . Finally we used a less extreme open model OCDM with  $\Omega_0 = 0.5$  which promises realistic large scale galaxy clustering, and which has the same mass variance at  $8h^{-1}\text{Mpc}$  as galaxies. All information about the models can be found in Table 1 and the corresponding power spectra are plotted in Fig 1.

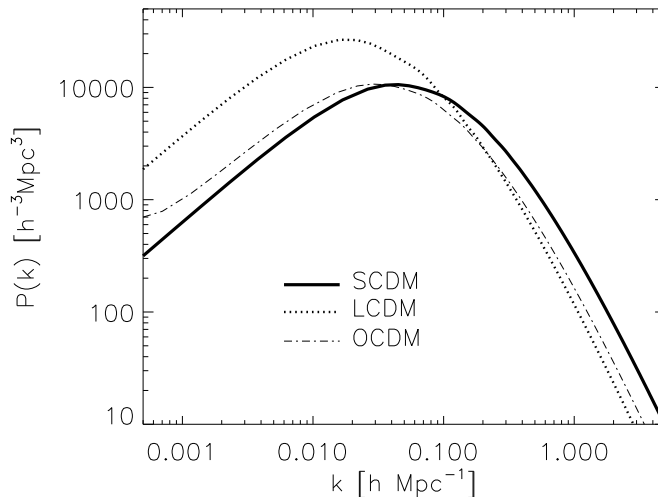


Figure 1: Power spectra for the models specified in Table 1

### 3 Numerical Techniques

#### 3.1 *N*-body simulations

To set up the numerical simulation of a gravitating system of dark matter particles one has to impose density fluctuations onto a distribution that represents a homogeneous and isotropic universe. Therefore a glass-like distribution is used for producing a starting realization (White 1993). To give an impression of the improvement using glass starting places as input for the following numerical simulation I have plotted in Fig 1 a slide through the initial particle distributions, using grid starting places and glass starting places, respectively. It can easily be seen that the input power spectrum is much better represented using the glass data.

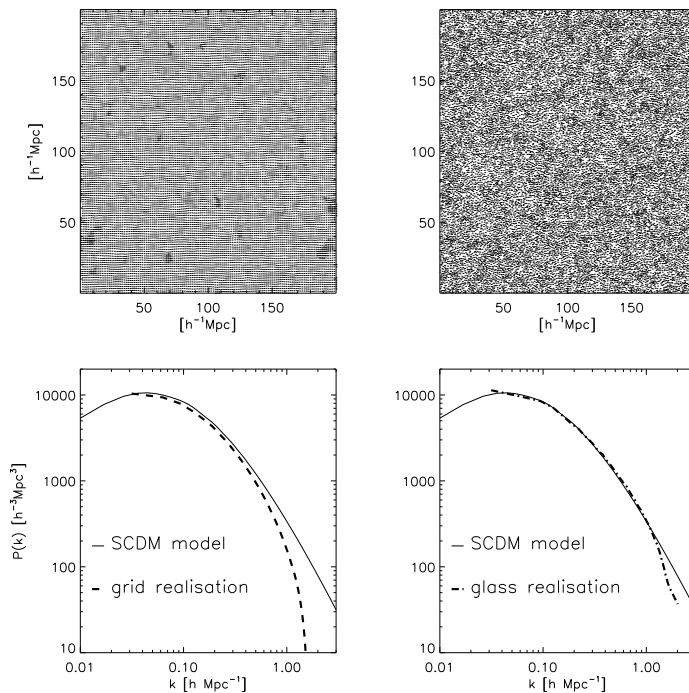


Figure 2: Representation of the initial power spectrum (SCDM model) using grid starting places (left panel) and glass starting places (right panel), respectively.

The evolution of the initial particle distribution is simulated using a modified version of the adaptive P<sup>3</sup>M code (Couchman 1991) which is able to allow

Table 2: Linking lengths  $l$  for the different models used with the friends-of-friends algorithm and the percentage of identified unvirialized particle groups.

|                                | $l$  | $\delta_{\text{TH}}$ | unvirialized halos |
|--------------------------------|------|----------------------|--------------------|
| <b>SCDM</b>                    | 0.20 | 178                  | 6 %                |
| <b><math>\Lambda</math>CDM</b> | 0.16 | 334                  | 3 %                |
| <b>OCDM</b>                    | 0.17 | 278                  | 2 %                |

for background expansions other than the Einstein-de-Sitter universe. The adaptive part of the code counter balances the dramatic slowdown caused by direct summation over nearby particles by placing refinement grids at the high density regions as clustering evolves. The force calculation for particles belonging to these refinements is performed by the same P<sup>3</sup>M code on a finer grid with isolated boundary conditions.

### 3.2 Identification of galaxy clusters

Groups of galaxies and galaxy clusters are identified with groups of dark matter particles defined with a standard friends-of-friends algorithm (Davis et al.1985). This methods collects particles in groups whose spatial separation  $r_u$  is smaller than  $l$  (linking length) times the mean inter particle spacing  $\Delta x$ :

$$r_u \leq l \cdot \Delta x. \quad (1)$$

At this point the question of the appropriate value for the linking length  $l$  arises. This parameter should be chosen in order to identify gravitational bound objects in the simulations. If we assume spherical halos with an isothermal density profile  $\rho(r) \propto 1/r^2$  and the usual value for the linking length  $l = 0.2$  we will find objects with an overdensity of  $\delta = (\rho - \bar{\rho})/\bar{\rho} \approx 180$  or higher (Lacey & Cole 1994). This value corresponds to  $\delta_{\text{TH}} \approx 178$  calculated for virialized objects under the assumption of a spherically symmetric collapse in an Einstein-de Sitter universe. In order to get the correct linking lengths for gravitationally bound objects in open and  $\Lambda$ -universes, we use the following formula:

$$l(\delta_{\text{TH}}) = 0.2 \left( \frac{178}{\delta_{\text{TH}}(\Omega_0, \Omega_{\Lambda,0})} \right)^{1/3} \quad (2)$$

The values of  $l$  listed in Table 2 are based on eq. 2 where the values of  $\delta_{\text{TH}}(\Omega_0, \Omega_{\Lambda,0})$  are calculated from the formula found in Katayama (1996).

However, even though the theory tells us that we should get virialized objects with a mean overdensity as given above, we cannot be sure that the particle groups we find by using the linking lengths from Table 2 in our friends-of-friends scheme are really physically virialized objects. In order to check this I have explicitly tested the virial theorem  $|E_{\text{pot}}| = 2 E_{\text{kin}}$  for each individual halo.

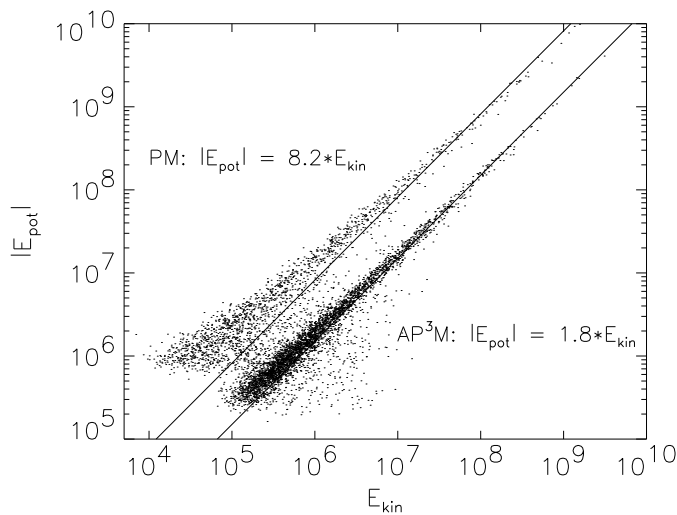


Figure 3: Virial theorem for clusters in the  $\Lambda$ CDM model (units are arbitrary).

Fig. 3 shows the virial relation as a scatter plot for all particle groups identified in the  $\Lambda$ CDM model at a redshift of  $z = 0$ . To emphasize the importance of high (spatial) resolution we have calculated the same model with a PM code that was run with exactly the same starting configuration as used for the AP<sup>3</sup>M code. The velocity dispersions in the PM simulation are throughout underestimated and lead to a correlation of the order  $|E_{\text{pot}}| \approx 8.2 E_{\text{kin}}$ . The 'lower' virial relation found in the AP<sup>3</sup>M simulation,  $|E_{\text{pot}}| \approx 1.8 E_{\text{kin}}$ , can be understood as an influence of an outer pressure of radially infalling particles into the halos (Cole & Lacey 1996). The obvious bend of the virial relation at low energies towards smaller  $E_{\text{kin}}$  proves that the surface influence decreases for groups of small particle numbers and the expected behaviour  $|E_{\text{pot}}| \approx 2 E_{\text{kin}}$  is reached. An opposite effect concerns a much smaller number of groups with velocity dispersions which are too high compared to their potential energy. These clusters are considered unvirialized and gave rise to question what ef-

fects are responsible for this deviation from virial equilibrium. Therefore they are treated separately in the following analysis, and are investigated in detail. Table 2 also shows the percentage of unvirialized objects among all FOF clusters for the different cosmological models. It becomes obvious that the percentage of unvirialized groups is highest in SCDM and lowest in OCDM. This is an representation of the different absolute abundance evolution in the different models.

#### 4 Properties of (un)virialized halos

One of the most basic properties of a galaxy cluster is its mass  $M$ . Therefore I would like to present the cumulative massfunction  $dn/dM$  in comparison to the prediction from the Press-Schechter theory (Press & Schechter 1974) and to observational data compiled by Bahcall & Cen (1993).

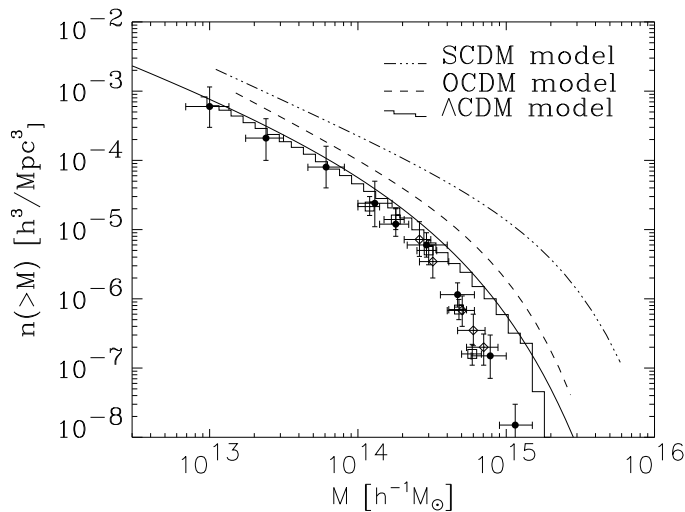


Figure 4: Axis ratio of virialized (dots) and unvirialized groups (diamonds) for the  $\Lambda$ CDM-simulation at  $z = 0$ .

Fig. 4 shows that the  $\Lambda$ CDM model best fits the observation and is very close to the prediction made by Press & Schechter. The PS curves for the SCDM and OCDM are left out for clarity; they match the numerical as well as the  $\Lambda$ CDM model.

In the following the nature of the unvirialized halos will be investigated in more detail.

First of all I will discuss the consequences of merger events for the shape of the resulting groups. To this aim the eigenvalues of the inertia tensor for each FOF group are calculated, which are given in the order  $a > b > c$ . In Fig. 5 we show a scatter plot of the ratios of the eigenvalues for the  $\Lambda$ CDM-simulation at  $z = 0$ . In this plot, spherical groups are situated near the origin, oblate clusters in the upper part and prolate clusters in the lower right corner. It is well know (Dubinsky 1992, Warren et al.1992, Lacey & Cole 1994) that hierarchical clustering leads to triaxial ellipsoids with a typical axis ratio of 6:4:3. The unvirialized halos inhabit more the right part of the diagram, again characterizing the soft merging, i.e. the elongation of the groups due to tidal interaction of the progenitors which marks the direction of the encounters, and in some cases to an elongation of the clusters in a second direction due to non-central encounters. Typically unvirialized clusters have an axis ratio of 8:4:3.

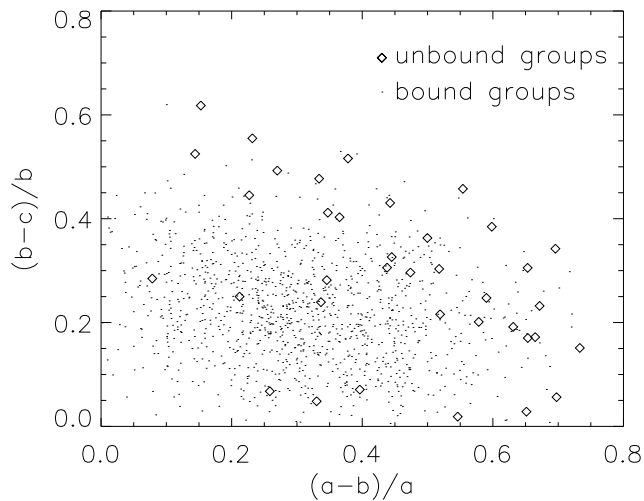


Figure 5: Axis ratio of virialized (dots) and unvirialized groups (diamonds) for the  $\Lambda$ CDM-simulation at  $z = 0$ .

Next I concentrate on the correlation of velocity dispersion and the mass of virialized and unbound groups. A tight correlation of both quantities for virialized objects is expected if we assume an isothermal sphere for the halo and a cutoff at constant density, which can easily be taken to be the mean cosmic density of the halos at the time when they form or suffer their last big merger. Since most halos form quite recently this cutoff is almost constant,

and we get

$$\sigma_v = V_c/\sqrt{2} \propto M^{\frac{1}{3}}. \quad (3)$$

As can be seen from Fig. 6 this is represented very well in our simulations with a large scatter for the light clusters. Fig. 6 also suggests that the unbound halos mostly lie at the low mass end of the distribution with high inner velocity dispersion. Cole & Lacey (1996) argue that the tail of groups with  $\sigma_v > V_c/\sqrt{2}$  are likely objects that belong to larger virialized structures. This may explain why we identify them as unvirialized objects. But if we repeat our analysis for objects obtained using a greater linking length  $l$  we derive the same results. Even for FOF groups identified with a linking length corresponding to an overdensity  $\delta \gg \delta_{\text{TH}}$  we find unbound groups in the tail  $\sigma_v > V_c/\sqrt{2}$ .

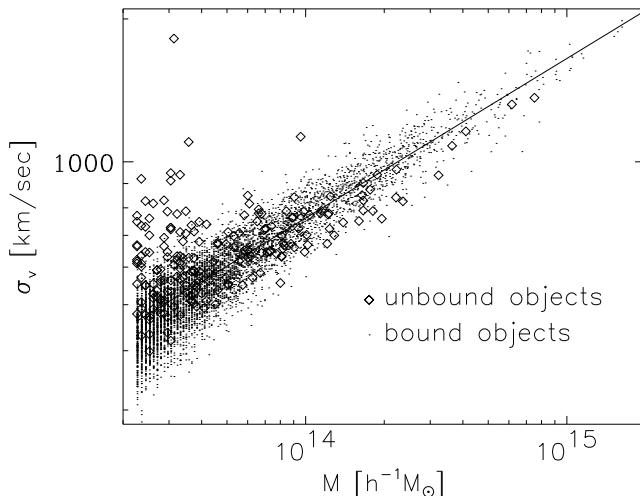


Figure 6: Relation between velocity dispersion and the mass for the  $\Lambda$ CDM model. The virialized halos are marked with points and the objects that are not in virial equilibrium are marked using diamonds. The solid line is a fit to the scaling relation  $\sigma_v \propto M^{\frac{1}{3}}$ .

More interesting than these low mass groups are the small number of halos lying beneath the virial relation  $\sigma_v = V_c/\sqrt{2}$ . They represent groups in the process of merging which are unbound because they are too extended. In most cases they represent halos with more than one centre which are connected by slight tidal bridges and similar structures. These systems are not very frequent, i.e. they do not survive for a long time, but they mark most interesting places in the simulation box. And it can be expected that they are sites for active



structure formation processes in nature. Fig. 8 (at the end of this article) shows the most massive unvirialized cluster in the  $\Lambda$ CDM simulation at  $z = 0.1$  and its two almost equal mass progenitors at  $z = 0.2$ . Both these progenitors are virialized objects just like the final merger product at a redshift of  $z = 0$ .

## 5 Correlation functions

One of the basic constraints of cosmological models is the shape and the amplitude of the two-point correlation function. For many years it has been the standard way to describe the clustering of galaxies and galaxy clusters. The assumption that galaxies (and clusters) only form from high-density regions above some threshold value  $\delta_c$  leads to a correlation of points exceeding this value  $\delta_c$  that is enhanced in comparison to the dark matter correlation function (Kaiser 1984).

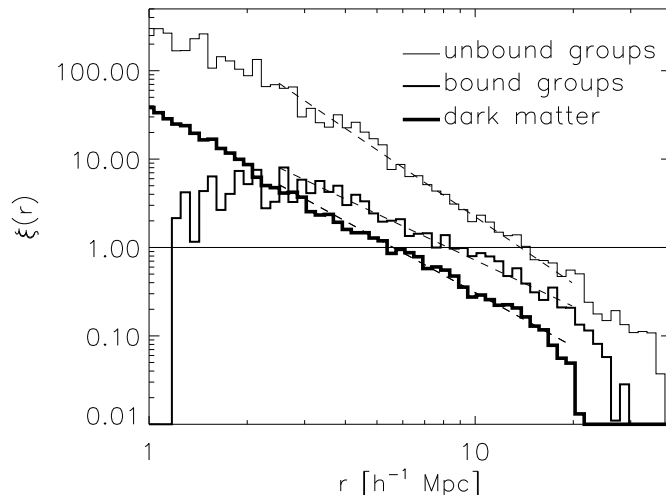


Figure 7: Correlation functions for the  $\Lambda$ CDM model. Histograms from below (at  $r > 3h^{-1}\text{Mpc}$ ) denote dark matter particles, virialized clusters and unvirialized groups, both with a mass cut corresponding to 50 particles. The dashed lines are fits with parameters specified in Table 3.

In Fig. 7 we show the correlation functions for the  $\Lambda$ CDM model. We find that the correlation between virialized groups containing more than 50 particles corresponding to a mass cut of  $4 \cdot 10^{13} h^{-1}M_{\odot}$  lies by a factor two over the correlation function of dark matter. We fitted standard power laws

Table 3: Fit parameter of the correlation functions for dark matter (first column), bound clusters (second column) and unbound clusters (third column) for three cosmological models.

|                                | dark matter |          | bound groups |          |      | unbound groups |          |
|--------------------------------|-------------|----------|--------------|----------|------|----------------|----------|
|                                | $r_0$       | $\gamma$ | $r_0$        | $\gamma$ | $N$  | $r_0$          | $\gamma$ |
| <b>SCDM</b>                    | 5.4         | 2.3      | 6.6          | 1.8      | 800  | 9.2            | 2.5      |
| <b><math>\Lambda</math>CDM</b> | 5.6         | 2.0      | 9.3          | 1.7      | 2200 | 13.8           | 2.5      |
| <b>OCDM</b>                    | 4.5         | 2.2      | 7.9          | 2.0      | 2200 | 11.4           | 2.5      |

$$\xi(r) = (r_0/r)^\gamma \quad (4)$$

which are shown in the Fig. 7 as dashed lines. Galaxy groups in the  $\Lambda$ CDM model have a correlation length  $r_0 \sim 9 h^{-1}\text{Mpc}$  and a slope  $\gamma = 1.7$ . The correlation function turns negative beyond  $30 h^{-1}\text{Mpc}$ . Fits for the other models are given in Table 3. To get comparable values for the different cosmologies we fixed the cluster number density to  $n = 10^{-5} h^3 \text{Mpc}^{-3}$  and used only the  $N = nV$  most massive clusters for the calculation of the correlation function. Obviously the amplitude in SCDM and OCDM are smaller than in the  $\Lambda$ CDM model, i.e., these models have too small power on large scales for describing the clustering of groups and clusters of galaxies.

The correlation function of the unvirialized groups is also of interest. They are much more strongly clustered than the virialized objects. Also the slope of the correlation function is very steep,  $\gamma = 2.5$ , independent of the cosmological model, cp. Table 3. This verifies that mergers are occurring at particular places in the universe, and that these processes are highly correlated. A similar result has been found for ultraluminous IRAS galaxies (Gao 1993).

## 6 Conclusions

We have collected a number of reasons for looking at virialization as a reasonable criterion for identifying groups and clusters of galaxies in numerical simulations. The virial theorem well described an overwhelming majority of the halos in our simulations. A slight bend in the virial relation can be ascribed to the effective pressure of the permanent spherical accretion stream in the halos. Special attention has been devoted to the unvirialized halos. We have shown that they are characterized by quite recent soft mergers which lead to more anisotropic halos and are strongly correlated over scales of up to  $40 h^{-1}\text{Mpc}$ . In our simulations we find a very fast virialization of the halos which leads to the small percentage of such objects at any given time. It

must be checked whether the virialisation time depends on the relatively low mass resolution in our big simulation boxes. The stronger anisotropy of the merger products leads to typical triaxial ellipsoids with axis ratios of 8:4:3. The merging processes are characterized by basically central encounters. Not much angular momentum is transferred to the merger product which leads to a self-similar growth of the rotation of the halos, (e.g. Knebe 1998).

The large differences in the correlation functions of the models makes it worthwhile to further compare differences in the large-scale matter distributions of the different models.

1. Bahcall N.A., Cen R., ApJ Lett. **407**, L49 (1993)
2. Bunn E.F., White M., ApJ **480**, 6 (1997)
3. Colberg J.M., White S.D.M., Jenkins A., Pearce F.R., astro-ph/9711040
4. Cole S., Lacey C., MNRAS **281**, 716 (1996)
5. Couchman H.M.P., ApJ **368**, L23 (1991)
6. Davis M., Efstathiou G., Frenk C. S., White S.D.M., ApJ **292**, 371 (1985)
7. Dubinski J., ApJ **401**, 441 (1992)
8. Einasto J., Einasto M., Tago E., Starobinsky A.A., Atrio-Baradela F., Müller V., Knebe A., Frisch P., Cen R., Andernach H., ApJ submitted (1997)
9. Gao Y., NASA Conf. Pub. 3190, p.54-55 (1993)
10. Kaiser N., ApJ Lett. **284**, L9 (1984)
11. Katayama T., Soto Y., ApJ **469**, 480 (1996)
12. Knebe A., in: Large Scale Structures: Tracks and Traces. Proceedings of the 12th Potsdam Cosmology Workshop, ed. V. Müller et al., World Scientific 1998, p. 175
13. Knebe A., Müller V., submitted to A&A (1998)
14. Lacey C., Cole S., MNRAS **271**, 676 (1994)
15. Peacock J. A., Dodds S.J., MNRAS **280**, 1020 (1996)
16. Press W.H., Schechter P., ApJ **187**, 425 (1974)
17. Seljak U., Zaldarriaga M., ApJ **469**, 437 (1996)
18. Warren M.S., Quinn P.J., Salmon J.K., Zurek W.H., ApJ **399**, 405 (1992)
19. White S.D.M., Les Houches Summer School 1993
20. White S.D.M., Efstathiou G., Frenck C.S., MNRAS **262**, 1023 (1993)

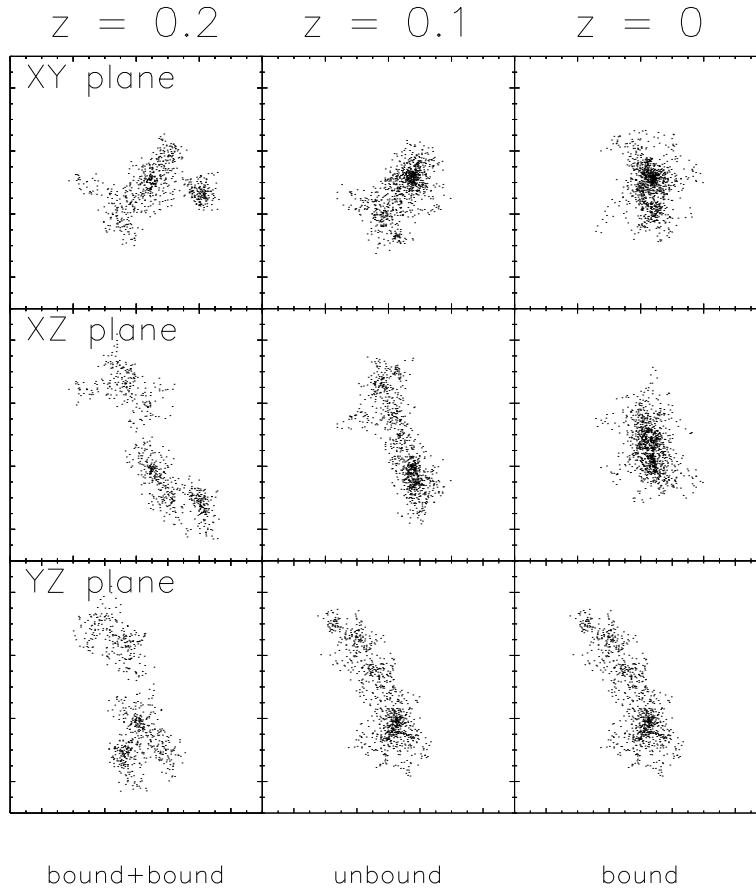


Figure 8: Projections of a cube of  $(10h^{-1}\text{Mpc})^3$  of the  $\Lambda\text{CDM}$  simulation box at redshifts  $z = 0.2$ ,  $z = 0.1$  and  $z = 0$ , containing the most massive unvirialized cluster. Only the particles in the cluster and in the two most massive progenitors are shown which are both virialized objects.